

RMNAS: A Multimodal Neural Architecture Search Framework For Robust Multimodal Sentiment Analysis

Haiyang Sun^{1,2}, Zheng Lian^{1,2}, Licai Sun^{1,2}, Bin Liu^{1,2}, Jianhua Tao³

School of Artificial Intelligence, University of Chinese Academy of Sciences¹

Chinese Academy of Sciences²

Department of Automation, Tsinghua University³

Abstract

Multimodal sentiment analysis (MSA) finds extensive applications, but the presence of missing modalities in real-world environments requires researchers to enhance the robustness of models, often demanding significant efforts. Multimodal neural architecture search (MNAS) is a more efficient approach. However, current MNAS methods, while effective in integrating multi-level information, are incapable of simultaneously searching for optimal operations to extract modality-specific information. This weakens the robustness of the model in addressing diverse scenarios. Moreover, these methods also fall short in enhancing the capture of emotional cues. In this paper, we propose robust-sentiment multimodal neural architecture search (RMNAS) framework. Specifically, we utilize the Transformer as a unified architecture for various modalities and incorporate a search for token mixers to enhance the encoding capacity of individual modalities and improve robustness across diverse scenarios. Subsequently, we leverage BM-NAS to integrate multi-level information. Furthermore, we incorporate local sentiment variation trends to guide the token mixers computation, enhancing the model's ability to capture sentiment context. Experimental results demonstrate that our approach outperforms or competitively matches existing state-of-the-art approaches in incomplete multimodal learning, both in sentence-level and dialogue-level MSA tasks, without the need for knowledge of incomplete learning.

Introduction

Multimodal Sentiment Analysis (MSA) aims to analyze the emotional states of users through the use of multiple modalities. Both sentence-level and dialogue-level MSA have found extensive applications in areas such as social media analysis (Somandepalli et al. 2021; Stappen et al. 2023) and human-computer interaction (Cambria 2016; Poria et al. 2017). While numerous studies have achieved promising results in MSA when dealing with complete modalities (Tsai et al. 2019; Hazarika, Zimmermann, and Poria 2020; Xue et al. 2020; Yu et al. 2021; Han, Chen, and Poria 2021), real-world scenarios introduce various challenges that impact the collection of multimodal data. Factors such as background noise in speech, obstacles in images, and recognition errors in text can lead to the omission of modal information. Without integrating insights from incomplete learning, these methods tend to exhibit vulnerabilities when con-

fronted with incomplete data. Consequently, various approaches have been proposed to bolster model robustness in these situations (Yuan et al. 2012; Li et al. 2018; Zhang et al. 2022; Tran et al. 2017; Zhao, Li, and Jin 2021; Lian et al. 2023; Sun et al. 2023c). However, this process is time-consuming and resource-intensive, as researchers need to invest significant time and resources in learning domain knowledge and testing various network structures. How can we address this problem more intelligently and efficiently?

Neural architecture search (NAS) presents a promising solution. By delineating task objectives and the search space, networks can autonomously uncover the optimal architecture for complete or incomplete scenarios, facilitated by search algorithms. However, current multimodal neural architecture search (MNAS) methods exhibit certain limitations. For instance, approaches like MMnas (Yu et al. 2020b) and MMIF (Peng et al. 2020) do not incorporate the fusion of multi-level information, despite its varying significance (Pepino, Riera, and Ferrer 2021). On the other hand, while methods like MFAS (Pérez-Rúa et al. 2019) and BM-NAS (Yin, Huang, and Zhang 2022) seek multi-level fusion strategies, they require predefined backbones for modality encoding, restricting their ability to find the optimal single-modality data encoding architectures across diverse scenarios. Moreover, these methods also fall short in enhancing the capture of emotional cues, thereby limiting their capacity to fully exploit sentiment information.

In order to address the aforementioned issues, we present the first MNAS framework for MSA, called robust-sentiment multimodal neural architecture search (RMNAS). Inspired by the MetaFormer (Yu et al. 2022; Yang et al. 2022), we employ the Transformer (Vaswani et al. 2017) as a unified backbone and conduct independent searches to identify optimal token mixers for each modality. This approach aims to liberate MNAS from the constraints of backbones, enabling the model to explore optimal encoding architectures for single-modality in various scenarios. Additionally, considering the dependence of emotional information on contextual cues (Lian, Liu, and Tao 2021), we introduce a novel fusion of sentiment trends with distance matrices to generate local sentiment variation trends (*LST*). These trends are subsequently employed to guide the token mixing process (Ying et al. 2021), enhancing RMNAS's capacity to comprehend emotional context. Lastly, we utilize

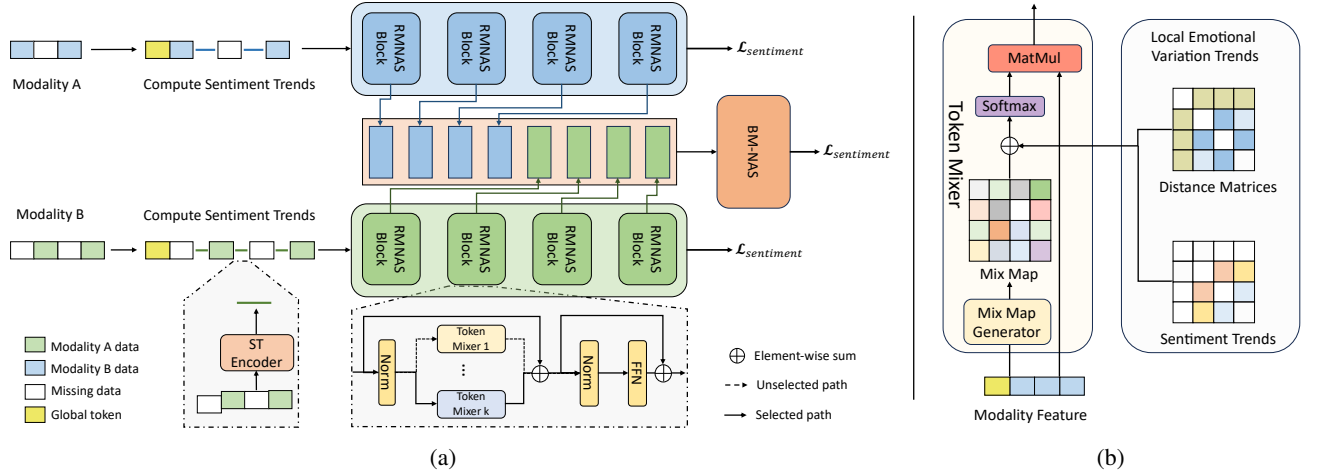


Figure 1: The overall framework of RMNAS. **In Figure 1(a)**, taking two modalities as an example, the modal information is first encoded by STEncoder to generate sentiment trends, which, along with the distance matrices, guides the calculation of token mixers. Subsequently, RMNAS blocks search for optimal token mixers for modality data encoding, while BM-NAS searches for the optimal fusion strategy for multi-level information. Each single-modal branch and the BM-NAS branch calculate the loss simultaneously to optimize the entire framework. **Figure 1(b)** shows how the **token mixer** internally generates the mix map. It combines local sentiment variation trends, which are composed of sentiment trends and the distance matrices, for guidance.

BM-NAS to search for the optimal strategy in fusing multi-level multimodal information.

To validate the effectiveness of our approach, we conduct experiments on multiple sentence-level and dialogue-level MSA tasks using a unified model config. Experimental results demonstrate that RMNAS achieves highly robust performance in incomplete multimodal learning, without the need for domain-specific knowledge, resulting in significant savings in resources. The main contribution of this paper can be summarized as follows:

- We design the first MNAS framework for MSA, named RMNAS. It can search for the optimal single-modality encoding architecture and multi-level multimodal information fusion strategy suitable for diverse scenarios.
- We encode local sentiment variation trends to guide the mixing process of the token mixer, enabling the model to robustly capture emotional information.
- Experimental results demonstrate that RMNAS achieves state-of-the-art or competitive performance without the need for knowledge of incomplete learning.

Related Work

Robust Multimodal Sentiment Analysis

Multimodal sentiment analysis (MSA) aims to utilize multiple modalities to understand the user’s emotional state. Most existing works focus on effectively mining heterogeneous information to enhance fusion performance. For instance, several works such as TFN (Xue et al. 2020), MISA (Hazrika, Zimmermann, and Poria 2020), Self-MM (Yu et al. 2021) and MMIM (Han, Chen, and Poria 2021) focus on utterance-level fusion. These studies utilize fusion operations such as simple concatenation, attention, and tensor-

based fusion to capture and integrate complete multimodal information. In addition, such as MulT (Tsai et al. 2019) and TFR-Net (Yuan et al. 2021) focus on fusing multimodal information at the element-level by leveraging the attention properties. However, in real-world deployment scenarios, multimodal information is often incomplete. Therefore, enhancing the robustness of models is of utmost importance. Some approaches (Yuan et al. 2012; Li et al. 2018) partition incomplete data into multiple subsets with complete modalities. CCA (Hotelling 1992; Andrew et al. 2013) and DC-CAE (Wang et al. 2015) aim to ensure strong correlation between low-dimensional representations of different modalities. CPM-Net (Zhang et al. 2022), MMIN (Zhao, Li, and Jin 2021) and (Sun et al. 2023c) aim to estimate missing information. Additionally, GCNet (Lian et al. 2023) explores enhancing the robustness of model in dialogue-level tasks.

However, the development of these approaches requires a significant amount of resource costs. In contrast, RMNAS achieves sota or competitive performance in incomplete multimodal learning without the need for knowledge of incomplete learning.

Multimodal Neural Architecture Search

Approaches like (Wu et al. 2022; Rajapakshe et al. 2023; Sun et al. 2023a,b) utilize NAS for extracting emotional information from speech, yet they are unable to handle multimodal data. There are some works focusing on constructing highly generalized multimodal neural architecture search (MNAS) methods. MMnas (Yu et al. 2020b) aims to search for optimal encoding and decoding operations for multimodal tasks, while MMIF (Peng et al. 2020) searches a CNN network that processes multiple modalities simultaneously. However, these methods can not effectively integrate multi-

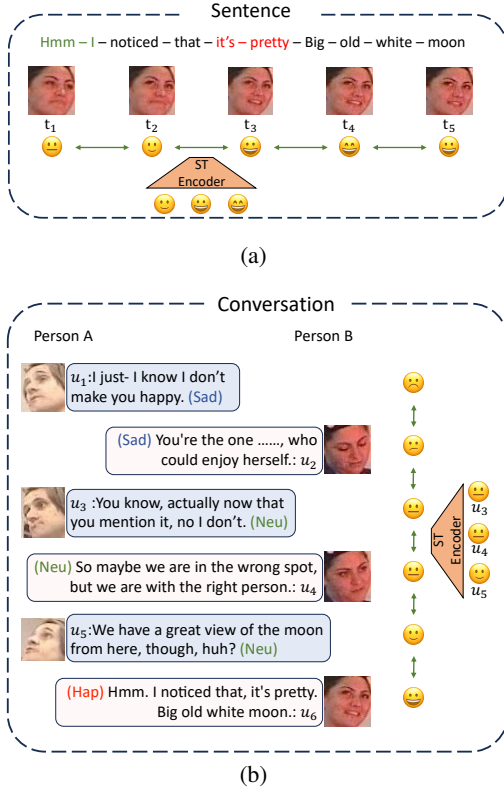


Figure 2: STEncoder extracts the sentiment trends.

level information. Although MFAS (Pérez-Rúa et al. 2019) and BM-NAS (Yin, Huang, and Zhang 2022) address this issue, they need predefined backbones to encode modalities, which imposes rigid constraints, restricting the model’s robustness to face various scenarios.

Method

In this section, we present the specific framework of RM-NAS. As illustrated in Figure 1, RMNAS consists of three main steps. Firstly, inspired by Graphormer (Ying et al. 2021), we capture the local sentiment variation trends (LST) for each feature node by incorporating the sentiment trends and distance matrices. Secondly, we construct the RMNAS block, which utilizes Transformer as the backbone and searches for the optimal token mixers for each modality, with LST guiding the mixing process. Finally, we employ BM-NAS to search for multi-level multimodal information fusion strategy. In addition to using the fused multimodal features to compute the task-specific loss \mathcal{L} , we calculate \mathcal{L} for each unimodal branch.

Input Format

In dialogue-level tasks, a conversation $C = \{(u_i, y_i^c)\}_{i=1}^{L_c}$ consists of L_c utterances, and the i^{th} utterance u_i with a label y_i^c . For each utterance, we extract features $x_m^c \in \mathbb{R}^{1 \times D_m}$ from modality $m \in \{\text{audio}, \text{video}, \text{text}\}$, where D represents the feature dimension, and concatenate them in the or-

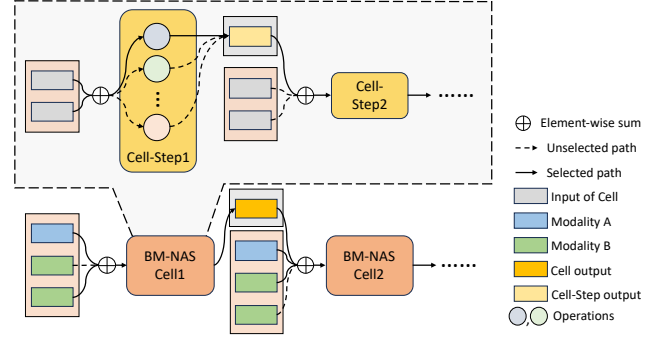


Figure 3: The search process of BM-NAS we used.

der of the dialogue to obtain $X_m^c \in \mathbb{R}^{L_c \times D_m}$, to represent the entire dialogue. In sentence-level tasks, each sentence $S = (\{t_i\}_{i=1}^{L_s}, y_i^s)$ consists of L_s frames, has an individual label. We extract modality features $X_m^s \in \mathbb{R}^{L_s \times D_m}$ to represents the complete sentence.

For feature $X_m \in \mathbb{R}^{N \times D_m}$, where N represents the sequence length, we first add positional encoding $PE_m \in \mathbb{R}^{N \times D_m}$ to incorporate temporal information:

$$X_m^p = X_m + PE_m \quad (1)$$

Then, we concatenate X_m^p with a trainable embedding $gt \in \mathbb{R}^{1 \times D_m}$, acting as a global token:

$$F_m^0 = \text{Concat}([gt, X_m^p]) \quad (2)$$

Next, X_m will be additionally used to extract LST_m , while F_m^0 will be fed into RMNAS blocks for modeling.

Local Sentiment Variation Trends

As depicted in Figure 2, emotional transitions commonly exhibit gradual shifts rather than abrupt changes, such as the transformation from a calm to a joyful speaker shown in Figure 2(a), and the transition in conversation atmosphere from sadness to happiness illustrated in Figure 2(b). The current emotional state of a speaker is closely connected to the emotional context of preceding and subsequent time points. For instance, the joyful emotion at t_2 and t_4 implies that the speaker at t_3 is likely to be happy. Furthermore, this connection diminishes as the time distance increases; for instance, the sad emotion of u_1 may not necessarily persist until u_6 . In order to enable the model to perceive such trends, we treat each frame’s features as time nodes, and combine sentiment trends (ST) with node distance matrices (DM) to create the local sentiment variation trends (LST), which serve as guidance for the interaction of feature nodes.

Sentiment Trends As shown in Figure 2, when extracting the ST between t_2 and t_3 , we use a 1DConv operation to combine the feature nodes of t_2 , t_3 , and t_4 , representing the trend of information changes, denoted as $st_{2-3} \in \mathbb{R}^{1 \times D_{lst}}$. The same approach can also be applied to extract the ST between u_3 and u_4 . We can extract st between all pairs of adjacent feature nodes using the same approach. Sentiment trends between non-adjacent pairs of nodes are obtained by

Algorithm 1: Pseudo code of LST Extraction.

Input: $X_m \in \mathbb{R}^{N \times D_m}$, $maxdis$
 ## $maxdis$ represents the maximum perceptual distance for each node.
Output: $LST_m \in \mathbb{R}^{(N+1) \times (N+1) \times D_{lst}}$

$STEncoder_m = \text{Conv1d}(D_m, D_{lst}, k, p = k//2, s = 1)$
 ## k, p , and s represent *kernelsize*, *pooling*, and *stride* respectively.
 $DisEncoder_m = \text{Linear}(1, D_{lst})$
 ## Utilized for encoding absolute distances.

$AST_m = STEncoder_m(X_m)[1:]$
 ## AST only contains the st between each pair of adjacent nodes.
 $ST_m = \text{Zeros}(N + 1, N + 1, D_{lst})$
 $DM_m = \text{Zeros}(N + 1, N + 1, D_{lst})$
 ## There are $N + 1$ tokens with the global token and feature nodes.

for i in $range(1, N + 1)$ **do**
for j in $range(i, N + 1)$ **do**
 $Path, Dis = \text{FindPath}(X_m[i - 1], X_m[j - 1])$
 ## Compute the shotest path and distance for each pair of feature nodes.
 $ST_m[i][j] = \text{Avg}(AST_m[p] \text{ for } p \text{ in } Path)$
 $DM_m[i][j] = -\text{inf}$ if $Dis > maxdis$ else $DisEncoder_m(Dis)$
 $ST_m[j][i], DM_m[j][i] = ST_m[i][j], DM_m[i][j]$
end for
end for

$DM_m[0][:] = DisEncoder_m(-1)$
 $DM_m[:,0] = DisEncoder_m(-1)$
 ## The distance between the global token and all feature nodes is uniformly as -1.
 $LST_m = ST_m + DM_m$
Return: LST_m

averaging the st values present in the shotest path between them. For example:

$$st_{2-4} = \text{Avg}(st_{2-3}, st_{3-4}) \quad (3)$$

Without considering the global token, this approach enables us to acquire the $ST \in \mathbb{R}^{N \times N \times D_{lst}}$ between each pair of feature nodes.

Distance Matrices To enhance the model’s focus on local sentiment trends, we additionally encode the absolute distances between each pair of nodes to obtain the $DM \in \mathbb{R}^{(N+1) \times (N+1) \times D_{lst}}$. It’s important to note that we treat the distance between the global token and all feature nodes as uniform and unique. Additionally, for node pairs that are too distant, we encode their $dm \in DM$ as negative infinity to prevent direct information interaction.

Finally, the ST and DM are fused to form the LST , which guides the calculation of the token mixers. Algorithm 1 provides the pseudo-code of LST extraction.

RMNAS Block

In RMNAS blocks, following the guidance of MetaFormer, we retain the overall structure of the Transformer but conduct a search for the token mixer selection for the input F_m^0 , as shown in Figure 1(a). Specifically, there are four operations in our token mixer search pool O_t : RAttentionMixing, RRandomMixing, RPoolMixing and RIdentityMixing. We assign a trainable weight $\alpha^i \in \mathbb{R}^4$ to O_t^i within the i^{th} block and use differentiable method to search for the optimal structure of each block. The encoding process of F_m^{i-1} in the i^{th}

block is as follows:

$$H_m^{i-1} = \text{LN}(F_m^{i-1}) \quad (4)$$

$$H_m^i = \sum_{o_t^i \in O_t^i} \frac{\exp(\alpha_{o_t^i}^i)}{\sum_{o_t^{i'} \in O_t^i \exp(\alpha_{o_t^{i'}}^i)} o_t^i(H_m^{i-1}) + F_m^{i-1}} \quad (5)$$

$$F_m^i = \text{FFN}(\text{LN}(H_m^i)) + H_m^i \quad (6)$$

where LN represents the layer normalization, FFN represents the feed-forward block.

As shown in Figure 1(b), to enhance the perception of emotional information within token mixers, the LST guides their process of generating the mixing map. Our token mixer computation process can be defined as follows:

- RAttentionMixing(H_m):

$$MixMap = \frac{(H_m W_q)(H_m W_k)^T}{\sqrt{d_{qk}}} + LST_m \quad (7)$$

$$OutPut = (H_m W_v) \otimes \text{Softmax}(MixMap) \quad (8)$$

where W_q, W_k and W_v are trainable parameters.

- RRandomMixing(H_m):

$$MixMap = RM + LST_m \quad (9)$$

$$OutPut = H_m \otimes \text{Softmax}(MixMap) \quad (10)$$

where RM is a frozen matrix after random initialization.

- RPoolMixing(H_m):

$$OutPut = \text{AvgPool}(H_m^T)^T - H_m \quad (11)$$

where AvgPool represents the average 1D pooling operation with $kernelsize = 3$.

- RIdentityMixing(H_m):

$$OutPut = H_m \quad (12)$$

BM-NAS

As shown in Figure 3, BM-NAS is proposed by (Yin, Huang, and Zhang 2022), and it composes of multiple Cells and Cell-Steps. BM-NAS comprises two categories of search pools. One category is utilized to select the input for Cells and Cell-Steps, denoted as O_c . The other category is employed to choose the encoding operations within the j^{th} Cell-Step of the i^{th} Cell, denoted as $O_s^{(i,j)}$. The O_c consists of two operations:

- $Identity(X) = X$, indicates that the feature is selected.
- $Zero(X) = 0$, indicates that the feature is unselected.

Each $O_s^{(i,j)}$ comprises five operations: Zero, Sum, Attention, LinearGLU, and ConcatFC. The detailed calculation process for these operations is described in the appendix. Assuming there are N_c candidates in hidden feature set H_c , BM-NAS assigns a trainable weight $\beta^k \in \mathbb{R}^{(N_c) \times 2}$ to control k^{th} input selection process. The calculation process for input X_k proceeds as follows:

$$X_k = \sum_{h_c \in H_c} \sum_{o_c \in O_c} \frac{\exp(\beta_{o_c}^k)}{\sum_{o_c' \in O_c} \exp(\beta_{o_c'}^k)} o_c(h_c) \quad (13)$$

The trainable weight $\lambda^{(i,j)}$ is allocated to control the selection of operations in $O_s^{(i,j)}$, and the calculation process is similar to Equation 13. It’s important to note that each Cell initially receives the input duplicated as two copies.

Table 1: Sentence-level performance comparison on CMU-MOSI and CMU-MOSEI in the incomplete modality setting. We report the AUILC of each evaluation metric under the missing rates of $\{0.0, 0.1, \dots, 1.0\}$. Performance provided by the paper of (Sun et al. 2023c). The best performance is highlighted in bold.

Models	Year	CMU-MOSI						CMU-MOSEI					
		MAE(\downarrow)	Corr(\uparrow)	Acc-7(\uparrow)	Acc-5(\uparrow)	Acc-2(\uparrow)	F1(\uparrow)	MAE(\downarrow)	Corr(\uparrow)	Acc-7(\uparrow)	Acc-5(\uparrow)	Acc-2(\uparrow)	F1(\uparrow)
MISA	2020	1.202	0.405	25.7	27.4	63.7	58.8	0.698	0.514	45.1	45.7	75.7	74.0
Self-MM	2021	1.162	0.444	27.8	30.3	67.5	66.2	0.685	0.507	46.7	47.3	75.4	72.9
MMIM	2021	1.168	0.450	27.0	29.4	66.9	65.8	0.694	0.502	45.9	46.4	72.4	69.3
TFR-Net	2021	1.156	0.452	27.7	30.5	67.8	66.1	0.689	0.511	46.9	47.3	74.2	73.4
EMT-DLFR	2023	1.106	0.486	32.5	35.6	70.3	70.3	0.665	0.546	47.9	48.8	76.9	75.9
RMNAS	Our	1.054	0.582	29.9	36.2	75.8	75.3	0.575	0.639	51.8	52.6	80.2	79.2

Table 2: Sentence-level performance comparison on CH-SIMS under the missing rates of $\{0.0, 0.1, \dots, 0.5\}$.

Models	Year	MAE(\downarrow)	Corr(\uparrow)	Acc-5(\uparrow)	Acc-3(\uparrow)	Acc-2(\uparrow)	F1(\uparrow)
MISA	2020	0.293	0.053	10.6	26.4	34.8	28.9
Self-MM	2021	0.231	0.258	18.3	30.5	37.4	37.5
MMIM	2021	0.244	0.238	17.7	29.8	37.0	36.2
TFR-Net	2021	0.236	0.253	17.8	30.0	37.3	37.2
EMT-DLFR	2023	0.215	0.287	20.4	31.9	38.4	38.5
RMNAS	Our	0.220	0.285	20.5	30.7	36.6	36.9

Table 3: Dialogue-level average WAF comparison on IEMOCAP, CMU-MOSI and CMU-MOSEI under the missing rates of $\{0.0, 0.1, \dots, 0.7\}$. Performance provided by the paper of (Lian et al. 2023).

Models	Year	IEMOCAP (four-class)	IEMOCAP (six-class)	CMU-MOSI	CMU-MOSEI
AE	2007	58.29	39.13	71.61	79.56
DCCAE	2015	51.87	36.03	58.92	70.05
MMIN	2021	64.91	47.15	72.92	78.54
CPM-Net	2022	51.46	35.32	67.77	72.52
GCNet	2023	75.20	56.18	76.75	83.76
RMNAS	Our	75.93	57.32	75.58	83.00

Architecture Search

In RMNAS, we have three types of parameters that control the variation of network structures: α , which controls the token mixer selection in each block; β , which controls the input selection for each Cell and Cell-Step; and λ , which controls the operation selection within each Step. During the training phase, two optimizers are employed to separately optimize model weights and $\{\alpha, \beta, \lambda\}$. The pseudo-code of our search method is provided in the appendix.

Experiments

Datasets

To validate the effectiveness of RMNAS, following previous works (Lian et al. 2023; Sun et al. 2023c), we conducted experiments on four benchmark datasets at both the sentence-level and dialogue-level MSA, including CH-SIMS (Yu et al. 2020a), CMU-MOSI (Zadeh et al. 2016), CMU-MOSEI (Zadeh et al. 2018), IEMOCAP (Busso et al. 2008). Detailed information are provided in the appendix.

Evaluation Metrics

Sentence-level Following (Sun et al. 2023c), in the training stage, we use mean absolute error (MAE) as the loss function and the metric for selecting the best model on the validation set. For CMU-MOSI and CMU-MOSEI, we report seven-class accuracy (Acc-7), five-class accuracy (Acc-5), binary accuracy (Acc-2), F1-score, MAE, and Pearson correlation coefficient (Corr) on test set. For CH-SIMS, we report ACC-5, ACC-3, Acc-2, F1-score, MAE, and Corr. Accuracy is calculated by evenly dividing continuous values into multiple intervals. Acc-2 and F1-score are computed by excluding the impact of samples with label 0.

Dialogue-level Following (Lian et al. 2023), for CMU-MOSI and CMU-MOSEI, we use MAE as the loss function and select the model based on the best weighted average F1-score (WAF) on the validation set, reporting its WAF on the test set. For IEMOCAP, we adopt a 5-fold leave-one-session strategy and report the mean of the best WAF on the test sets. WAF is computed by excluding the samples with label 0.

Experiments Setup

We conduct experiments on all datasets using a unified setting, incorporating three modalities: text, audio, and video. The kernel size of the *STEncoder* is set to 7, and *maxdis* is set to 8. Each unimodal data is encoded through 6 RMNAS blocks. Each block has a hidden dimension of 448, an FFN hidden layer ratio of 4.0, and GAttentionMixing with 8 head nums. There are 2 Cells in BM-NAS, and each Cell contains 2 Cell-Steps with a fusion feature dimension of 240. The model weights are optimized using AdaW with a learning rate of $5e-4$, and α, β, λ are optimized using SGD with a learning rate of 5. The model is trained using a batch size of 32 for 100 epochs, with an additional early stopping mechanism of 8 epochs for the Sentence-level tasks. We run each model three times and report average results.

Results

Comparison to State-of-the-art

Overall Scenario Performance Since the data missing rate is often not fixed in real-world scenarios, considering the overall performance under various missing rates is an important indicator for the robustness. Following prior work, for sentence-level tasks (Sun et al. 2023c), we compute the area under indicators line chart (AUILC) for each metric.

Table 4: Sentence-level performance comparison on CMU-MOSI and CMU-MOSEI under a 70% missing rate. Performance provided by the author of (Sun et al. 2023c). The best performance is highlighted in bold.

Models	Parameters	CMU-MOSI						CMU-MOSEI					
		MAE(↓)	Corr(↑)	Acc-7(↑)	Acc-5(↑)	Acc-2(↑)	F1(↑)	MAE(↓)	Corr(↑)	Acc-7(↑)	Acc-5(↑)	Acc-2(↑)	F1(↑)
MISA	110.6M	1.386	0.185	19.1	19.3	52.4	58.5	0.754	0.457	41.2	41.5	73.4	73.4
Self-MM	109.9M	1.373	0.260	18.3	19.2	60.7	61.0	0.754	0.445	42.3	42.7	72.9	73.3
MMIM	109.8M	1.335	0.308	18.6	19.4	59.5	45.8	0.759	0.385	42.7	42.8	70.0	65.5
EMT-DLFR	110.5M	1.266	0.364	26.8	29.0	65.1	65.3	0.724	0.485	44.8	45.3	73.9	73.3
RMNAS	63.8M	1.014	0.646	32.4	38.5	77.7	77.7	0.577	0.645	51.7	52.5	79.9	78.5

Table 5: Sentence-level performance comparison on CH-SIMS under a 50% missing rate.

Models	Parameters	MAE(↓)	Corr(↑)	Acc-5(↑)	Acc-3(↑)	Acc-2(↑)	F1(↑)
MISA	110.6M	0.590	0.197	21.7	53.3	69.4	81.4
Self-MM	109.9M	0.509	0.418	31.3	55.5	70.5	70.8
MMIM	109.8M	0.518	0.399	27.8	53.8	69.2	68.0
EMT-DLFR	110.5M	0.451	0.541	37.3	60.3	73.5	73.3
RMNAS	63.8M	0.453	0.540	42.1	63.6	72.9	73.2

Table 6: Dialogue-level WAF comparison on IEMOCAP, CMU-MOSI and CMU-MOSEI under a 70% missing rate. Performance provided by the paper of (Lian et al. 2023).

Models	Parameters	IEMOCAP	IEMOCAP	CMU-MOSI	CMU-MOSEI
		(four-class)	(six-class)		
CPM-Net	-	44.76	31.25	61.79	67.07
AE	1.3M	39.86	23.18	55.64	72.81
MMIN	3.9M	55.44	37.84	61.53	71.18
GCNet	10.7M	71.38	53.46	68.35	80.20
RMNAS	63.8M	73.28	55.79	66.05	79.64

Assuming there are some results denoted as $(mr_i, p_i)_{i=1}^{L_p}$, where mr represents the missing rate and p represents the metric, the calculation of AUILC can be formulated as:

$$AUILC = \sum_{i=0}^{L_p-1} \frac{1}{2} (p_i + p_{i+1}) (mr_{i+1} - mr_i) \quad (14)$$

As shown in Tables 1 and 2, on both CMU-MOSI and CMU-MOSEI datasets, RMNAS demonstrates a clear advantage, achieving the best performance in metrics of MAE, Corr, Acc-5, Acc-2, and F1. Notably, compared to current sota method EMT-DLFR, RMNAS demonstrates substantial enhancements in Corr, Acc-2, and F1 metrics, achieving increments of 0.096, 5.5%, and 5% respectively on CMU-MOSI, and 0.093, 3.3%, and 3.3% respectively on CMU-MOSEI. On the CH-SIMS dataset, RMNAS performs slightly less favorably than EMT-DLFR but closely, and it outperforms other approaches. EMT-DLFR enhances the model’s robustness in missing scenarios by reconstructing low- and high-level features, and effectively utilizes the pre-trained BERT model through fine-tuning. Without specific design for missing scenarios, RMNAS outperforms EMT-DLFR on CMU-MOSI and CMU-MOSEI datasets, while maintaining comparable performance on CH-SIMS.

For dialogue-level tasks (Lian et al. 2023), we calculate the average performance across various missing rates.

As shown in Table 3, on the IEMOCAP dataset, RMNAS surpasses the current sota method GCNet, achieving improvements of 1.9% and 2.33% in the four-class and six-class tasks, respectively. On CMU-MOSI and CMU-MOSEI datasets, RMNAS performs slightly weaker than GCNet but closely, and outperforms other approaches. GCNet enhances model robustness by reconstructing low-level features and modeling speaker information. Without being specifically designed for dialogue scenarios, RMNAS surpasses GCNet on the IEMOCAP dataset and maintains comparable performance on CMU-MOSI and CMU-MOSEI datasets.

The above results demonstrate that, without the need for incorporating incomplete learning knowledge, RMNAS leverages its ability to search for optimal architectures under varying missing rates, encompassing both sentence-level and dialogue-level tasks, and achieves sota or competitive performance. This highlights the significant advantage of MNAS in addressing incomplete learning challenges and underscores the strong performance of RMNAS.

Severe Missing Scenarios Performance To comprehensively assess the robustness of RMNAS, we further compare the performance of various methods in severe missing scenarios. For sentence-level tasks, table 4 presents the performance of each model at a 70% missing rate in CMU-MOSI and CMU-MOSEI datasets. It is evident that RMNAS exhibits significant robustness. For instance, on CMU-MOSI, our approach achieves remarkable improvements of 0.282 in Corr, 9.5% in Acc-5, 12.6% in Acc-2, and 12.4% in F1 metrics. Table 5 demonstrates the performance of different methods with a 50% missing rate on CH-SIMS dataset. Our method is slightly weaker in MAE, Corr, Acc-2, and F1 metrics compared to EMT-DLFR, yet the performance is remarkably close. Combining the findings from Table 1 and 2, it becomes apparent that the superiority of our method in AUILC is primarily driven by its outstanding performance in sentence-level severe missing scenarios. Conversely, EMT-DLFR leverages its extensive model training parameters to achieve better performance in mild missing data scenarios.

For dialogue-level tasks, Table 6 presents the performance of different methods on the IEMOCAP, CMU-MOSI, and CMU-MOSEI datasets under a 70% missing rate. Similar to the earlier results, RMNAS demonstrates superior performance on the IEMOCAP dataset, while it slightly lags behind GCNet on the remaining datasets. This also reaffirms the robustness of our approach in dialogue-level tasks.

In the appendix, we present the results for all missing rates. These results further validate the remarkable robust-

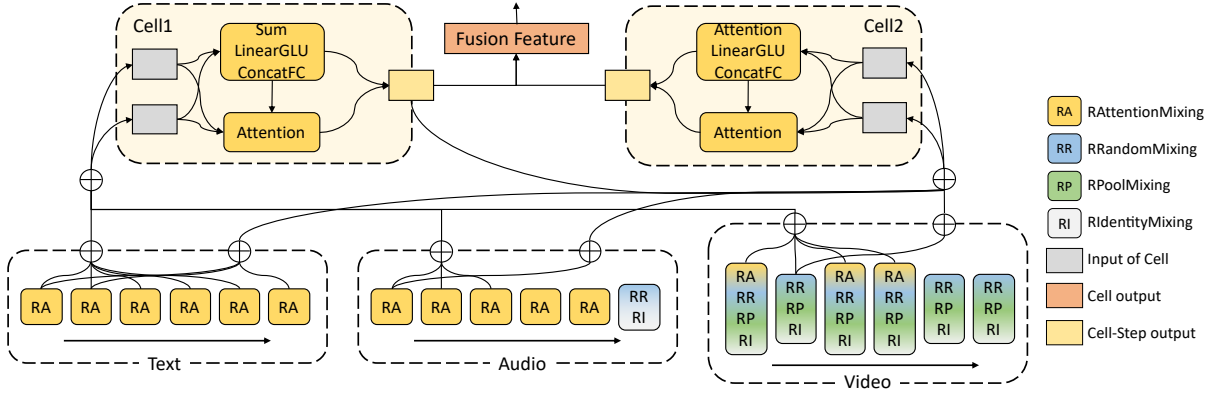


Figure 4: The optimal architecture on the CH-SIMS dataset with a 50% missing rate. Operations with α, β, γ less than 0.2 after softmax computation are considered discarded.

Table 7: Ablation study on different modules in RMNAS, conducted on the CH-SIMS dataset with a 50% missing rate.

LST	Mixer Search	Retrain	MAE(\downarrow)	Corr(\uparrow)	Acc-3(\uparrow)	F1(\uparrow)
×	×	×	0.479	0.494	57.9	70.2
✓	×	×	0.470	0.505	59.0	72.7
✓	✓	×	0.465	0.507	59.4	72.8
✓	✓	✓	0.453	0.540	63.6	73.2

ness of RMNAS in scenarios involving data incompleteness.

Ablation Study

Different Modules To verify the significance of *LST* in capturing emotional information and the importance of the RMNAS block for model robustness, we perform a comparative study of different model architectures on the CH-SIMS dataset under a missing rate of 50%. The results are shown in Table 7. It’s evident that the incorporation of *LST* significantly enhances the model’s ability to discern emotions, leading to improvements in all performance metrics. However, while the integration of token mixer search allows the exploration of optimal encoding structures for individual modalities, the expanded search space introduces randomness during training, which hampers the effective optimization of model weights. As a result, the performance gains are not significant. Retraining the model weights from scratch addresses this issue, leading to further improvements in model performance, ultimately achieving the best results. The optimal architecture searched by RMNAS is shown in Figure 4. It can be observed that the encoding operations for different modalities vary significantly, with video modality particularly requiring more complex architectures to extract modality-specific information. This underscores the importance of searching for single-modality encoding operations to enhance model robustness.

Limitations of BM-NAS To fairly illustrate the limitations of BM-NAS in MSA, we conduct experiments by integrating it with sota methods. The entire model is trained

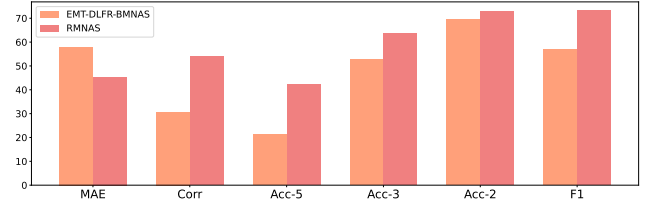


Figure 5: Ablation study on different unimodal encoders, conducted on the CH-SIMS dataset with a 50% missing rate. The MAE and Corr have been scaled by a factor of 100.

from scratch on the CH-SIMS dataset with a missing rate of 50%. Using the same setup, we employ BM-NAS to search for fusion strategy for multi-level information in EMT-DLFR, denoted as EMT-DLFR-BMNAS. The results, depicted in Figure 5, underscore the superiority of RMNAS across all evaluation metrics. This highlights the necessity of searching for single-modal encoding operations when dealing with incomplete data. Solely searching for fusion strategy would weaken the model’s robustness across various scenarios. Moreover, the performance of RMNAS signifies its ability to excel beyond EMT-DLFR in single-modal encoding, even though the RMNAS block is not specifically designed for any particular modality. On the other hand, due to the necessity of predefined single-modal backbones in BM-NAS, it is not compatible with networks such as GC-Net that employ early fusion strategy.

Conclusion

In this paper, we propose the first MNAS framework for MSA, named RMNAS. It enables the simultaneous search for single-modal encoding operations and multi-level multimodal information fusion strategy while effectively capturing emotional information. Experimental results demonstrate that RMNAS surpasses or competitively matches existing sota methods in incomplete multimodal learning, across both sentence-level and dialogue-level MSA tasks, without requiring knowledge of incomplete learning.

References

- Andrew, G.; Arora, R.; Bilmes, J.; and Livescu, K. 2013. Deep canonical correlation analysis. In *International conference on machine learning, ICML*, 1247–1255. PMLR.
- Busso, C.; Bulut, M.; Lee, C.; Kazemzadeh, A.; Mower, E.; Kim, S.; Chang, J. N.; Lee, S.; and Narayanan, S. S. 2008. IEMOCAP: interactive emotional dyadic motion capture database. *Lang. Resour. Evaluation*, 42(4): 335–359.
- Cambria, E. 2016. Affective Computing and Sentiment Analysis. *IEEE Intell. Syst.*, 31(2): 102–107.
- Han, W.; Chen, H.; and Poria, S. 2021. Improving Multimodal Fusion with Hierarchical Mutual Information Maximization for Multimodal Sentiment Analysis. In *Proceedings of the 2021 Conference on Empirical Methods in Natural Language Processing, EMNLP*, 9180–9192.
- Hazarika, D.; Zimmermann, R.; and Poria, S. 2020. Misa: Modality-invariant and-specific representations for multimodal sentiment analysis. In *Proceedings of the ACM International Conference on Multimedia, ACM MM*, 1122–1131.
- Hotelling, H. 1992. Relations between two sets of variates. In *Breakthroughs in statistics: methodology and distribution*, 162–190. Springer.
- Li, Y.; Yang, T.; Zhou, J.; and Ye, J. 2018. Multi-Task Learning based Survival Analysis for Predicting Alzheimer’s Disease Progression with Multi-Source Block-wise Missing Data. In *Proceedings of the 2018 SIAM International Conference on Data Mining, SDM*, 288–296.
- Lian, Z.; Chen, L.; Sun, L.; Liu, B.; and Tao, J. 2023. GCNet: Graph Completion Network for Incomplete Multimodal Learning in Conversation. *IEEE Trans. Pattern Anal. Mach. Intell, TPAMI*, 45(7): 8419–8432.
- Lian, Z.; Liu, B.; and Tao, J. 2021. CTNet: Conversational Transformer Network for Emotion Recognition. *IEEE ACM Trans. Audio Speech Lang. Process.*, 29: 985–1000.
- Peng, Y.; Bi, L.; Fulham, M. J.; Feng, D.; and Kim, J. 2020. Multi-modality Information Fusion for Radiomics-Based Neural Architecture Search. In *Medical Image Computing and Computer Assisted Intervention, MICCAI*, 763–771.
- Pepino, L.; Riera, P.; and Ferrer, L. 2021. Emotion Recognition from Speech Using wav2vec 2.0 Embeddings. In *INTERSPEECH*, 3400–3404.
- Pérez-Rúa, J.; Vielzeuf, V.; Pateux, S.; Baccouche, M.; and Jurie, F. 2019. MFAS: Multimodal Fusion Architecture Search. In *Proceedings of the IEEE/CVF Conference on Computer Vision and Pattern Recognition, CVPR*, 6966–6975.
- Poria, S.; Cambria, E.; Bajpai, R.; and Hussain, A. 2017. A review of affective computing: From unimodal analysis to multimodal fusion. *Inf. Fusion*, 37: 98–125.
- Rajapakshe, T.; Rana, R.; Khalifa, S.; Sisman, B.; and Schuller, B. 2023. Improving Speech Emotion Recognition Performance using Differentiable Architecture Search. *arXiv preprint arXiv:2305.14402*.
- Somandepalli, K.; Guha, T.; Martinez, V. R.; Kumar, N.; Adam, H.; and Narayanan, S. 2021. Computational Media Intelligence: Human-Centered Machine Analysis of Media. *Proc. IEEE*, 109(5): 891–910.
- Stappen, L.; Baird, A.; Schumann, L.; and Schuller, B. W. 2023. The Multimodal Sentiment Analysis in Car Reviews (MuSe-CaR) Dataset: Collection, Insights and Improvements. *IEEE Trans. Affect. Comput. TAC*, 14(2): 1334–1350.
- Sun, H.; Lian, Z.; Liu, B.; Li, Y.; Sun, L.; Cai, C.; Tao, J.; Wang, M.; and Cheng, Y. 2023a. EmotionNAS: Two-stream Architecture Search for Speech Emotion Recognition. In *INTERSPEECH*.
- Sun, H.; Zhang, F.; Lian, Z.; Guo, Y.; and Zhang, S. 2023b. MFAS: Emotion Recognition through Multiple Perspectives Fusion Architecture Search Emulating Human Cognition. *arXiv preprint arXiv:2306.09361*.
- Sun, L.; Lian, Z.; Liu, B.; and Tao, J. 2023c. Efficient multimodal transformer with dual-level feature restoration for robust multimodal sentiment analysis. *IEEE Transactions on Affective Computing, TAC*.
- Tran, L.; Liu, X.; Zhou, J.; and Jin, R. 2017. Missing Modalities Imputation via Cascaded Residual Autoencoder. In *Proceedings of the IEEE/CVF Conference on Computer Vision and Pattern Recognition, CVPR*, 4971–4980.
- Tsai, Y. H.; Bai, S.; Liang, P. P.; Kolter, J. Z.; Morency, L.; and Salakhutdinov, R. 2019. Multimodal Transformer for Unaligned Multimodal Language Sequences. In *Proceedings of the 57th Conference of the Association for Computational Linguistics, ACL*, 6558–6569.
- Vaswani, A.; Shazeer, N.; Parmar, N.; Uszkoreit, J.; Jones, L.; Gomez, A. N.; Kaiser, L.; and Polosukhin, I. 2017. Attention is All you Need. In *Advances in Neural Information Processing Systems, NIPS*, 5998–6008.
- Wang, W.; Arora, R.; Livescu, K.; and Bilmes, J. A. 2015. On Deep Multi-View Representation Learning. In *International conference on machine learning, ICML*, 1083–1092.
- Wu, X.; Hu, S.; Wu, Z.; Liu, X.; and Meng, H. 2022. Neural architecture search for speech emotion recognition. In *International Conference on Acoustics, Speech and Signal Processing, ICASSP*, 6902–6906. IEEE.
- Xue, H.; Yan, X.; Jiang, S.; and Lai, H. 2020. Multi-Tensor Fusion Network with Hybrid Attention for Multimodal Sentiment Analysis. In *International Conference on Machine Learning and Cybernetics, ICMMLC*, 169–174.
- Yang, L.; Hu, Y.; Lu, S.; Sun, Z.; Mei, J.; Han, Y.; and Li, X. 2022. Searching for BurgerFormer with micro-meso-macro space design. In *International Conference on Machine Learning, ICML*, 25055–25069. PMLR.
- Yin, Y.; Huang, S.; and Zhang, X. 2022. BM-NAS: Bilevel Multimodal Neural Architecture Search. In *AAAI Conference on Artificial Intelligence, AAAI*, 8901–8909.
- Ying, C.; Cai, T.; Luo, S.; Zheng, S.; Ke, G.; He, D.; Shen, Y.; and Liu, T.-Y. 2021. Do transformers really perform badly for graph representation? *Advances in Neural Information Processing Systems, NIPS*, 34: 28877–28888.

- Yu, W.; Luo, M.; Zhou, P.; Si, C.; Zhou, Y.; Wang, X.; Feng, J.; and Yan, S. 2022. Metaformer is actually what you need for vision. In *Proceedings of the IEEE/CVF conference on computer vision and pattern recognition, CVPR*, 10819–10829.
- Yu, W.; Xu, H.; Meng, F.; Zhu, Y.; Ma, Y.; Wu, J.; Zou, J.; and Yang, K. 2020a. CH-SIMS: A Chinese Multimodal Sentiment Analysis Dataset with Fine-grained Annotation of Modality. In *Proceedings of the 58th Annual Meeting of the Association for Computational Linguistics, ACL*, 3718–3727.
- Yu, W.; Xu, H.; Yuan, Z.; and Wu, J. 2021. Learning Modality-Specific Representations with Self-Supervised Multi-Task Learning for Multimodal Sentiment Analysis. In *AAAI Conference on Artificial Intelligence, AAAI*, 10790–10797.
- Yu, Z.; Cui, Y.; Yu, J.; Wang, M.; Tao, D.; and Tian, Q. 2020b. Deep Multimodal Neural Architecture Search. In *Proceedings of the ACM International Conference on Multimedia, ACM MM*, 3743–3752.
- Yuan, L.; Wang, Y.; Thompson, P. M.; Narayan, V. A.; and Ye, J. 2012. Multi-source feature learning for joint analysis of incomplete multiple heterogeneous neuroimaging data. *NeuroImage*, 61(3): 622–632.
- Yuan, Z.; Li, W.; Xu, H.; and Yu, W. 2021. Transformer-based Feature Reconstruction Network for Robust Multimodal Sentiment Analysis. In *Proceedings of the ACM International Conference on Multimedia, ACM MM*, 4400–4407.
- Zadeh, A.; Liang, P. P.; Poria, S.; Cambria, E.; and Morency, L. 2018. Multimodal Language Analysis in the Wild: CMU-MOSEI Dataset and Interpretable Dynamic Fusion Graph. In *Proceedings of the 56th Annual Meeting of the Association for Computational Linguistics, ACL*, 2236–2246.
- Zadeh, A.; Zellers, R.; Pincus, E.; and Morency, L. 2016. Multimodal Sentiment Intensity Analysis in Videos: Facial Gestures and Verbal Messages. *IEEE Intell. Syst.*, 31(6): 82–88.
- Zhang, C.; Cui, Y.; Han, Z.; Zhou, J. T.; Fu, H.; and Hu, Q. 2022. Deep Partial Multi-View Learning. *IEEE Trans. Pattern Anal. Mach. Intell, TPAMI*, 44(5): 2402–2415.
- Zhao, J.; Li, R.; and Jin, Q. 2021. Missing Modality Imagination Network for Emotion Recognition with Uncertain Missing Modalities. In *Proceedings of the 56th Annual Meeting of the Association for Computational Linguistics, ACL*, 2608–2618.